CWE-8
June 7-11, 2026
London, ON, Canada

Impact of Stoss Slope on Airflow Dynamics over Transverse Dunes in Deserts: Experimental and Numerical Investigations

Sumaja Kolli [a], Pradeep Kumar Dammala [b], Hassan Hemida [c]

[a] *Indian Institute of Technology Jodhpur, Jodhpur, Rajasthan, India, kolli.1@iitj.ac.in*
[b] *Indian Institute of Technology Jodhpur, Jodhpur, Rajasthan, India, pkdammala@iitj.ac.in*
[c] *University of Birmingham, Birmingham, United Kingdom, h.hemida@bham.ac.uk*

SUMMARY
The current study investigates airflow patterns over transverse dunes with varying stoss slopes (10°, 20°, and 32°) using a scaled model through experimental wind-tunnel and CFD studies. Velocity profiles and surface pressure distributions were measured to examine variations in flow acceleration, stagnation, and separation. CFD results agree well with experiments for dunes with 20° and 32° slopes, capturing velocity trends, pressure variation, and separation behaviour. Wind speed analysis revealed steeper stoss slopes intensify flow deceleration and enlarge the separation zone, while gentler slopes produce smoother acceleration and delayed separation. Surface pressure distributions supported these findings and reflected similar trends with 10° slope experiencing the highest negative pressure near crest.
Keywords: *Sand Dune, Wind Tunnel, Aeolian Erosion, Computational Fluid Dynamics*

1. INTRODUCTION

Windblown sand disrupts and inundates infrastructure, agricultural farmlands and causes severe environmental impacts. The extent of aeolian erosion is highly influenced by the morphology of sand dunes and wind flow patterns in the vicinity. Realizing the impact, many researchers since pioneering work of Bagnold (1941) delved into understanding aeolian erosion. Since sand dunes evolve continuously with time, their interaction with wind and surroundings keeps modifying, hence extensive work was done on understanding on influence of windward and leeward slopes on sand transport dynamics (Walker and Nickling, 2003; Parson et al., 2004; Dong et al., 2007, Faria et al., 2011, Kolli et al., 2026). Stoss slope plays a key role in governing near-surface acceleration, adverse pressure gradients near the crest, and the size of the lee-side recirculation zone, can therefore alter erosion potential and sediment transport pathways. Despite these advances, the specific role of variable stoss slopes in transverse dune aerodynamics remains insufficiently quantified, particularly under controlled laboratory conditions where dune height and lee slope are held constant. To address this gap, the present study investigates airflow dynamics over scaled transverse dunes with identical height and lee slope but systematically varied stoss slopes (10°-D10, 20°-D20, and 32°-D32). A combination of wind tunnel experiments and Reynolds-averaged Navier Stokes (RANS) based CFD simulations is employed to quantify wind speed variation, surface pressure distribution, and flow separation characteristics. The comparison between CFD and experimental data provides further insights into the reliability of RANS models in resolving shallow and steep dune slopes. The outcomes contribute to improved understanding of dune–flow interactions, with implications for aeolian erosion prediction, dune migration modeling, and desert infrastructure planning.

2. METHODOLOGY

2.1. Dune Models

Current study examines scaled dune models of varying stoss slopes (10°, 20° and 32°). All dunes share a common lee slope of 32° and a uniform height of 50 mm. The adopted dune model adheres to the similitude principles outlined by White (1996) and discussed in detail in Kolli et al. (2026). All the models are 3D printed representing old dunes that are immobilized in nature/stationary dunes with the identical lee slope, matching the angle of repose of soil particles of desert areas (Ferreira and Lambert, 2011; Kolli et al., 2023).

2.2. Experimental Setup

Experiments were carried out at the subsonic wind tunnel (WT) setup (0.6m x 0.6m x 4m at Indian Institute of Technology Jodhpur, India. The width of models is spanned across the complete width of WT representing a two-dimensional transverse dune. Single channel electronic manometer connected to the pitot static tube is utilized to measure the wind velocities. The streamwise velocity profile at 0.5m from outlet of empty WT matches power law approximation with an exponent (α) of 0.13 similar to the arid settings of White (1996) study on sand dunes, as shown in Figure 2(a). The power law curve is given by:

$$u_z/u_{ref} = (z/z_{ref})^{\alpha}, \quad \text{..... (1)}$$

Where u_z and u_{ref} are the streamwise velocities along at height z from the wind tunnel floor and at the reference height, $z_{ref} \approx 0.22$m beyond the boundary layer thickness of 0.18m, respectively. Further, surface pressure distribution across the dune is measured using 8 Port Surface Pressure Scanner system by Sunshine Pvt Ltd. Pressure taps were drilled and attached on the printed dune models. The resultant surface pressure is reported in terms of pressure coefficient as shown in Eq. (2).

$$C_p = \frac{p - p_\infty}{0.5\rho u_{ref}^2} \quad \text{..... (2)}$$

Here p is actual pressure at the surface pressure tap, p_∞ is the free stream (reference) pressure, and ρ represents the density of air.

2.3. Numerical Setup and Methodology

The current setup employs commercially available Computational Fluid Dynamics (CFD) code CFX (ANSYS, 2024) for numerical modelling. CFX utilizes finite volume discretization method to solve the 3D Reynolds Average Navier's Stokes (RANS) equation. Existing studies focusing on numerical modelling on aeolian sand transport reported reliable outputs based on RANS, validated by experimental wind tunnel investigations (Faria et al., 2011; Tominaga et al., 2018). A fully developed homogeneous turbulent state is planned to be considered where a standard k-ε model is employed to solve the corresponding Reynolds-averaged Navier-Stokes equations of motion. The numerical convergence is set to 10^{-5} for all the normalized residuals.

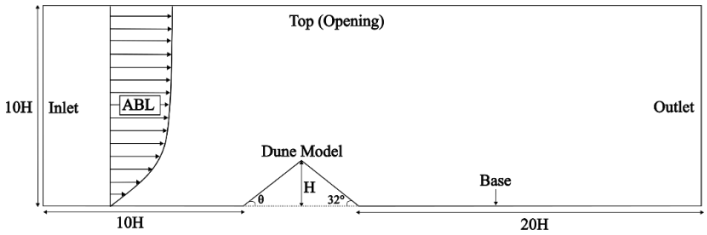

Figure 1 Dimensions of the Computational Domain

The size of the computational domain (refer Figure 1) is defined by the grid independence tests. The inflow in the computational domain is defined at the inlet with the velocity profile matching the wind tunnel inlet velocity profile as shown in Figure 1. The outflow is set to be fully developed conditioned and zero gradient with zero relative static pressure. The dune model, top and side walls of the computational domain are treated as wall with no slip condition. Further, the obtained results of simulations were validated by comparing the surface pressure readings of wind tunnel experiment with computational results.

3. RESULTS AND DISCUSSION

3.1. Wind Speed Characteristics

The wind speed variation with stoss slope is represented through wind speed up ratio presented in Figure 2(b). Wind speed up ratio is defined as $u_{z\theta}/u_z$ where $u_{z\theta}$ is the wind speed measured 1mm above dune surface along the slope at elevation z and u_z is the inlet wind speed without the dune model at same elevation.

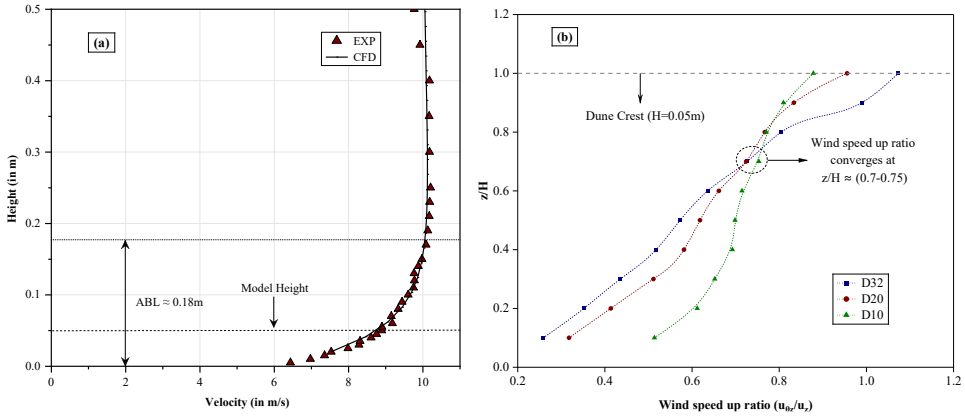

Figure 2. (a) Inlet wind velocity profile (b)Wind Speed up ratio along the stoss slope of D32 and D20

A generalised trend of increase in wind speed up ratio is noted as flow approaches towards the crest. Near to the toe of dune ($z/H < 0.4$), lowest speed-up ratio is exhibited by the steepest slope (D32) highlighting the stagnation effect induced by abrupt steeper slope. In contrast, gentler slopes (D10 and D20) with rather smoother transition maintain higher speed-up ratios at these initial stages. Beyond this z/H range i.e. at z/H of 0.4-0.7, rapid increase in speed up ratio is reported until z/H $\approx$ 0.7 and interestingly reported to have $u_{z\theta}/u_z$ converged at z/H of 0.7-0.75. While gentler slopes observed to increase smoothly toward the crest, D32 undergoes a sharper acceleration due to the compressed streamline curvature near the crest. Ultimately, D32 reaches the highest peak speed-up ratio, approaching or slightly exceeding unity, which corresponds to near-crest flow destabilization and the onset of flow separation immediately downstream.

3.2. Surface Pressure Distribution

Figures 3(a) and 3(b) depict the surface pressure coefficient (C_p) distribution on the stoss and lee sides of dune models respectively. All dune models reported a monotonic decrease in Cp as the wind flow on stoss ascends towards the dune crest. Lowest Cp values were reported by gentler slope (D10) reflecting its higher and more sustained acceleration along the windward face. In contrast, the steepest dune, D32, exhibits a noticeably milder reduction in C_p, indicating the influence of a stronger adverse pressure gradient that suppresses acceleration and increases flow resistance. These differences become most evident near the crest, where D32 attains the highest (least negative) $C_p$value, signifying weaker suction and a greater likelihood of flow detachment. D20 shows intermediate behavior, closely following the trend between D10 and D32.

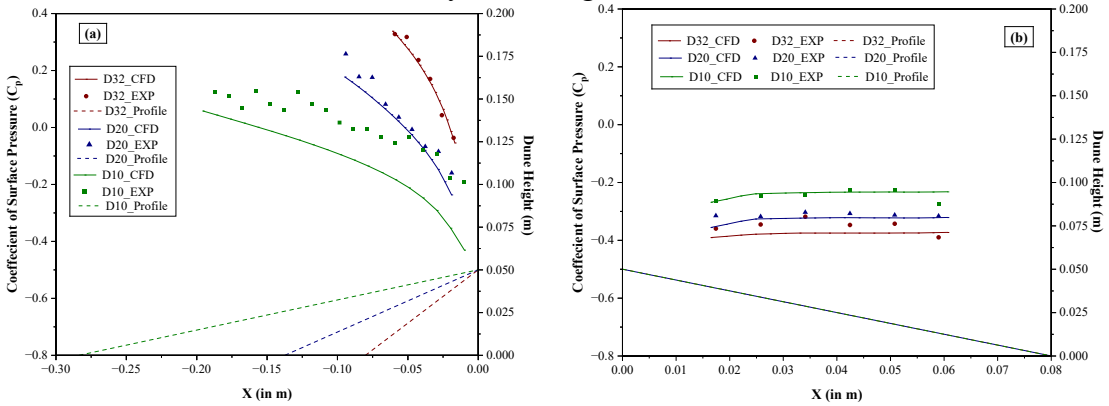

Figure 3 Variation of Cp at centre of dune along the length (a) Stoss side and (b) Lee side

The CFD predictions capture these patterns well, demonstrating good agreement in both the magnitude and slope-dependent ranking of the pressure distributions. A small deviation is noted for D10, where CFD slightly overpredicts the pressure drops on the stoss side. This is likely due to the challenges of resolving the thin, gradually accelerating boundary layer over the gentle slope and the tendency of incorporated model to overestimate streamline curvature. Nevertheless, both CFD and experiments exhibit consistent trends, indicating that the discrepancy affects only magnitude and not overall aerodynamic behavior. On the lee side, all dunes display a characteristic plateau in C_p, marking the presence of a separated shear layer and the associated recirculation zone. D32 produces the largest and deepest low-pressure region, followed by D20 and D10, consistent with the stronger separation tendency of steeper dunes.

4. CONCLUSIONS

Preliminary experimental wind tunnel and CFD studies were conducted on scaled dunes of varying stoss slope and constant lee slope. Wind speed-up measurements show that gentler slopes (D10, D20) promote smoother acceleration along the stoss surface, while the steepest slope (D32) induces initial stagnation followed by rapid near-crest acceleration. All dunes exhibit a consistent speed-up convergence around $z/H \approx 0.7 - 0.75$, marking a transition height beyond which the slope effect diminishes. Stoss-side pressure distributions mirror these trends, with D10 producing the most negative pressures and D32 experiencing a milder drop due to enhanced adverse pressure gradients. Minor deviations between CFD and experiments for D10 are attributed to challenges in modelling the thin, accelerating boundary layer over gentle slopes. On the lee side, all models display a distinct low-pressure plateau associated with flow separation, with the depth and reattachment length increasing systematically with

stoss-slope steepness. CFD results show strong agreement with experimental trends for both stoss and lee sides of D32 and D20, reliably capturing velocity profile, surface pressure distribution, separation behavior, and reattachment locations. This consistency indicates that the RANS-based numerical approach, when supported by an appropriate boundary-layer inflow specification, can reliably reproduce key aerodynamic features over dune geometries. Although the current investigation focuses on stationary dunes under unidirectional flow, future studies could incorporate mobile dune configurations and multidirectional wind conditions to further advance understanding of dune-flow interactions.

ACKNOWLEDGEMENTS

We thank the Commonwealth Scholarship Commission in the UK (CSC) for funding the academic visiting period at University of Birmingham, UK.

REFERENCES

Bagnold, R. A. 1941. The physics of blown sand and desert dunes. Boca Raton, FL: Chapman & Hall.

Parsons, D. R., Walker, I. J., & Wiggs, G. F. (2004). Numerical modelling of flow structures over idealized transverse aeolian dunes of varying geometry. Geomorphology, 59(1-4), 149-164.

Walker, I. J., & Nickling, W. G. (2003). Simulation and measurement of surface shear stress over isolated and closely spaced transverse dunes in a wind tunnel. Earth Surface Processes and Landforms: The Journal of the British Geomorphological Research Group, 28(10), 1111-1124.

Dong, Z., Qian, G., Luo, W., & Wang, H. (2007). A wind tunnel simulation of the effects of stoss slope on the lee airflow pattern over a two-dimensional transverse dune. Journal of Geophysical Research: Earth Surface, 112(F3).

Faria, R., Ferreira, A. D., Sismeiro, J. L., Mendes, J. C., & Sousa, A. C. (2011). Wind tunnel and computational study of the stoss slope effect on the aeolian erosion of transverse sand dunes. Aeolian Research, 3(3), 303-314.

Kolli, S., Bind, A., Dammala, P. K., & Hemida, H. (2026). Influence of sand dune geometry on aeolian erosion and dune migration: A wind tunnel study. Wind and Structures (In Press).

White, B. R. (1996). Laboratory simulation of aeolian sand transport and physical modeling of flow around dunes. Annals of Arid Zone, 35(3).

Dammala, P. K., Kolli, S., Garaga, R., Reddy, K. R., & Kumar, P. (2025). Aeolian sand dune fixation–critical review of measures, challenges and future perspectives with a case study on Thar Desert. CATENA , 250 , 108786.

Kolli, S., Dammala, P. K., Ul Haq, A., & Reddy, K. R. (2023). Valorization of Scrapped Marble Slurry Powder as Potential Sand Dune Stabilizer: Pilot Studies on Thar Desert Soils. Journal of Hazardous, Toxic, and Radioactive Waste, 27(4), 04023025.

Tominaga, Y., Okaze, T., & Mochida, A. (2018). Wind tunnel experiment and CFD analysis of sand erosion/deposition due to wind around an obstacle. Journal of Wind Engineering and Industrial Aerodynamics, 182, 262-271.